H_2O_2 induces nuclear transport of the receptor tyrosine kinase c-MET in breast cancer cells via a membrane-bound retrograde trafficking mechanism

Received for publication, September 21, 2018, and in revised form, March 27, 2019 Published, Papers in Press, April 8, 2019, DOI 10.1074/jbc.RA118.005953

Mei-Kuang Chen[‡§], Yi Du[§], Linlin Sun[§¶], Jennifer L. Hsu[§], Yu-Han Wang[§‖], Yuan Gao[§**], Jiaxing Huang[§‡‡], and Mien-Chie Hung[‡§‖§§1]

*From the [‡]The University of Texas MD Anderson Cancer Center UTHealth Graduate School of Biomedical Sciences and the [§]Department of Molecular and Cellular Oncology, The University of Texas M. D. Anderson Cancer Center, Houston, Texas 77030, the [¶]Tianjin Key Laboratory of Lung Cancer Metastasis and Tumor Microenvironment, Lung Cancer Institute, Tianjin Medical University General Hospital, Tianjin 300052, China, the [‖]Graduate Institute of Biomedical Sciences and [§§]Center of Molecular Medicine, China Medical University, Taichung 402, Taiwan, the **Department of General Surgery, Xinhua Hospital Affiliated to Shanghai Jiao Tong University School of Medicine, Shanghai 200092, China, and the [‡‡]Department of Medical Oncology, Cancer Center, West China Hospital, Sichuan University, Chengdu 610041, China*

Edited by Xiao-Fan Wang

Reactive oxygen species (ROS) are cellular by-products produced from metabolism and also anticancer agents, such as ionizing irradiation and chemotherapy drugs. The ROS H_2O_2 has high rates of production in cancer cells because of their rapid proliferation. ROS oxidize DNA, protein, and lipids, causing oxidative stress in cancer cells and making them vulnerable to other stresses. Therefore, cancer cell survival relies on maintaining ROS-induced stress at tolerable levels. Hepatocyte growth factor receptor (c-MET) is a receptor tyrosine kinase overexpressed in malignant cancer types, including breast cancer. Full-length c-MET triggers a signal transduction cascade from the plasma membrane that, through downstream signaling proteins, up-regulates cell proliferation and migration. Recently, c-MET was shown to interact and phosphorylate poly(ADP-ribose) polymerase 1 in the nucleus and to induce poly(ADP-ribose) polymerase inhibitor resistance. However, it remains unclear how c-MET moves from the cell membrane to the nucleus. Here, we demonstrate that H_2O_2 induces retrograde transport of membrane-associated full-length c-MET into the nucleus of human MCF10A and MCF12A or primary breast cancer cells. We further show that knocking down either coatomer protein complex subunit γ1 (COPG1) or Sec61 translocon β subunit (SEC61β) attenuates the accumulation of full-length nuclear c-MET. However, a c-MET kinase inhibitor did not block nuclear c-MET transport. Moreover, nuclear c-MET interacted with KU proteins in breast cancer cells, suggesting a role of full-length nuclear c-MET in ROS-induced DNA damage repair. We conclude that a membrane-bound retrograde vesicle transport mechanism facilitates membrane-to-nucleus transport of c-MET in breast cancer cells.

Reactive oxygen species (ROS)[2] are highly reactive molecules derived from oxygen metabolism mainly produced during metabolic processes, as well as from ionizing radiation (IR) and chemotherapy drugs (1). ROS can be grouped into either radical molecules, such as hydroxyl radical and superoxide anion, or nonradical compounds, such as H_2O_2, which plays a key role in physiological oxidative stress (2). Because ROS can lead to oxidation of macromolecules, including DNA, protein, and lipids, precise homeostasis control of ROS is crucial to both normal and cancer cells. A moderate level of ROS is important for physiological regulations but can also activate oncogenic signaling molecules, leading to human cancer initiation and progression (1, 3, 4). However, excessive ROS can also induce DNA damage and apoptosis in cancer cells (3). Therefore, enhancing ROS level is a strategy widely applied in cancer treatment (1, 3, 5). In cancer cells, the ROS H_2O_2 can be generated during ligand-induced receptor tyrosine kinase (RTK) activation and can further enhance RTK autophosphorylation by inhibiting protein-tyrosine phosphatase activity (6). In addition to the alteration of RTK signaling, ROS also enhances the accumulation of nuclear RTKs such as c-MET and epidermal growth factor receptor (EGFR) (7–10).

Nuclear RTKs are termed as membrane receptors in the nucleus (MRINs) (11), and MRINs can translocate into the

This work was supported in part by National Institutes of Health Grants P30 CA016672 and R01CA211615; 2015–2016 Scholarships for Excellence in Biochemistry and Molecular Biology at M. D. Anderson Cancer Center (to M.-K. C.); 2017–2018 Larry Deaven Ph.D. Fellowship in Biomedical Sciences (to M.-K. C.); Natural Science Foundation of Tianjin Grant 16JCYBJC24400 (to L. S.); National Natural Science Foundation of China Grant 31301160 (to L. S.); and funds from the China Scholarship Council (to L. S.). The authors declare that they have no conflicts of interest with the contents of this article. The content is solely the responsibility of the authors and does not necessarily represent the official views of the National Institutes of Health.
This article contains Figs. S1 and S2.

[1] To whom correspondence should be addressed: China Medical University, 91 Hsueh-Shih Rd., Taichung 40402, Taiwan. E-mail: mhung@mail.cmu.edu.tw.

[2] The abbreviations used are: ROS, reactive oxygen species; PARP, poly(ADP-ribose) polymerase; IR, ionizing radiation; RTK, receptor tyrosine kinase; EGFR, epidermal growth factor receptor; MRIN, membrane receptor in the nucleus; ER, endoplasmic reticulum; COPI, coat protein complex I; FGFR, fibroblast growth factor receptor; HGF, hepatocyte growth factor; TNBC, triple-negative breast cancer; BFA, brefeldin A; DMEM, Dulbecco's modified Eagle's medium; DAPI, 4′,6′-diamino-2-phenylindole; CTF, carboxyl-terminal fragment; AraC, 1-β-D-arabinofuranosylcytosine; STR, short tandem repeat.

nucleus via at least two main trafficking pathways: 1) RTK intracellular domains generated by γ-secretase cleavage are released into cell cytosol for direct translocation into nucleus, and 2) RTKs with intact transmembrane domains translocate into nucleus through a clathrin-mediated endocytic mechanism and then travel in a retrograde trafficking vesicle by a membrane-bound mechanism (12, 13). The retrograde membrane vesicle transport mechanism includes the trafficking from the Golgi body to endoplasmic reticulum (ER) where the coat protein complex I (COPI) vesicle is an essential carrier for MRIN transport between Golgi stacks and also carries MRINs from the Golgi to ER (14–16). After reaching the ER, the ER-to-nucleus transport of MRIN requires Sec61β (16, 17). However, there are also two mechanisms reported for ER-to-nucleus transport of MRIN: 1) integrative nuclear FGFR-1 signaling (INFS) for FGFR-1 and 2) INTERNET for EGFR (16, 18, 19). For the INFS pathway, FGFR-1 is pumped out from the ER and enters the cytosol before entering the nucleus through the nuclear pore complex, whereas for the INTERNET pathway, EGFR remains membrane-bound and is transferred from the ER membrane connecting to outer nuclear membrane, through nuclear pore complex and then into the inner nuclear membrane (13, 20). The exact mechanism by which the MRIN enters the nucleus from inner nuclear membrane is not yet clear. However, Sec61β in the inner nuclear membrane is required, and a membrane-associated vesicle is likely involved (16, 20).

Various RTKs are reported to shuttle from the plasma membrane into cell nucleus where they are known to have noncanonical functions in transcriptional regulation, DNA replication, and DNA repair regulation (9, 11, 12, 16, 21–26). c-MET is an RTK commonly activated in EGFR inhibitor–resistant cancer patients (27–30). Canonical full-length c-MET holoreceptor is a cell membrane RTK that is activated by its ligand hepatocyte growth factor (HGF), and the activation of c-MET holoreceptor is important for promoting cell proliferation, migration, and survival through the common RTK downstream messenger proteins, such as GAB1/Grb2, phosphatidylinositol 3-kinase, and STAT3 (31). Overexpression of c-MET has been observed in multiple cancer types, including triple-negative breast cancer (TNBC), and is highly correlated with poor prognosis and drug resistance in cancer patients (29, 30, 32–36). However, the biological function of c-MET is not limited to its canonical signaling role from plasma membrane. c-MET holoreceptor also translocates into the nucleus rapidly to initiate calcium signaling in liver cells upon HGF stimulation (37). Moreover, constitutively active cytosolic fragments of c-MET (MET-CTF) are present continuously in the nuclei of TNBC cell line MDA-MB-231 and involved in transcription regulation (38). Previously, we demonstrated that c-MET can translocate into nucleus to interact with and phosphorylates PARP1 in response to H_2O_2 stimulation, which contributes to PARP inhibitor resistance in TNBC (10).

In this study, we report that upon H_2O_2 stimulation, c-MET holoreceptor utilizes INTERNET pathway to translocate into the nucleus via the COPI/Sec61β-mediated retrograde vesicle trafficking. The H_2O_2-induced nuclear transport of c-MET occurs independently from c-MET phosphorylation. Moreover, we also show that nuclear c-MET can interact with KU proteins, which binds DNA double-strand breaks in DNA repair. Our findings suggested the involvement of H_2O_2-induced nuclear c-MET in DNA damage repair.

Results

ROS-induced nuclear full-length c-MET accumulates in breast cancer cells

To investigate whether full-length c-MET holoreceptor can translocate into the nucleus in response to ROS, we treated several c-MET–expressing cell lines derived from human mammary gland (MCF10A and MCF12A) or breast cancers with 10 mM H_2O_2 followed by cellular fraction and Western blotting to detect c-MET. We observed an accumulation of full-length c-MET in the nucleus for all cell lines tested after H_2O_2 treatment, whereas differential response to H_2O_2 treatment was observed for the truncated form of c-MET (MET-CTF) (Fig. 1*A*). We then further stimulated MDA-MB-231 and BT-549 cells with increasing concentrations of H_2O_2 and found that nuclear c-MET holoreceptor accumulation ocurred in a dose-dependent manner (Fig. 1*B*). Treatment of 1–10 mM H_2O_2 induced c-MET nuclear translocation. The concentration of H_2O_2 at 10 mM was used in our experimental setting to observe significant nuclear c-MET accumulation to study mechanisms of membrane receptor trafficking. This concentration has been shown to be sufficient to affect multiple physiology functions in mammalian cells including DNA damage (39, 40). Time-course experiments indicated that a 30-min H_2O_2 stimulation is sufficient for c-MET nuclear accumulation in both MDA-MB-231 and BT-549 cells (Fig. 1*C*). ROS inducing agents, such as doxorubicin, IR, and sodium arsenite, can also induce accumulation of full-length nuclear c-MET in breast cancer cells (Fig. 1, *D* and *E*, and Fig. S1), suggesting that c-MET nuclear translocation phenomenon is not limited to direct H_2O_2 treatment. On the contrary, chemotherapeutic agents that do not stimulate ROS accumulation, such as cisplatin and paclitaxel, did not induce nuclear c-MET accumulation (Fig. S1). We also found that prolonged ligand treatment (100 ng/ml HGF for 1–6 h) stimulated full-length nuclear MET accumulation in both MDA-MB-231 (1 h) and BT549 cells (6 h) (Fig. S2). Quantitative Western blotting analysis showed that full-length nuclear c-MET increased by 2-fold in MDA-MB-231 cells and by up to 7-fold in BT-549 cells (Fig. S2). However, unlike ligand-stimulated nuclear EGFR accumulation, which takes only within 30 min (18), nuclear accumulation of full-length c-MET takes at least 1 h after ligand stimulation (Fig. S2). Together, c-MET can translocate into the nucleus efficiently in response to different stimuli, but the ligand-induced translocation seems to be slower than that of EGFR.

To determine the number of cells that contained nuclear c-MET after HGF or H_2O_2 stimulation, we performed several experiments using MDA-MB-231 and BT-549 cells. Immunostaining of c-MET indicated that it mainly located in the cytosol under normal culture conditions (control). It also aggregated at the perinuclear and nuclear regions in response to either HGF or H_2O_2 stimulation. Quantitative confocal microscopy also showed increasing amounts of cells containing nuclear c-MET after H_2O_2 stimulation. Consistent with the results from West-

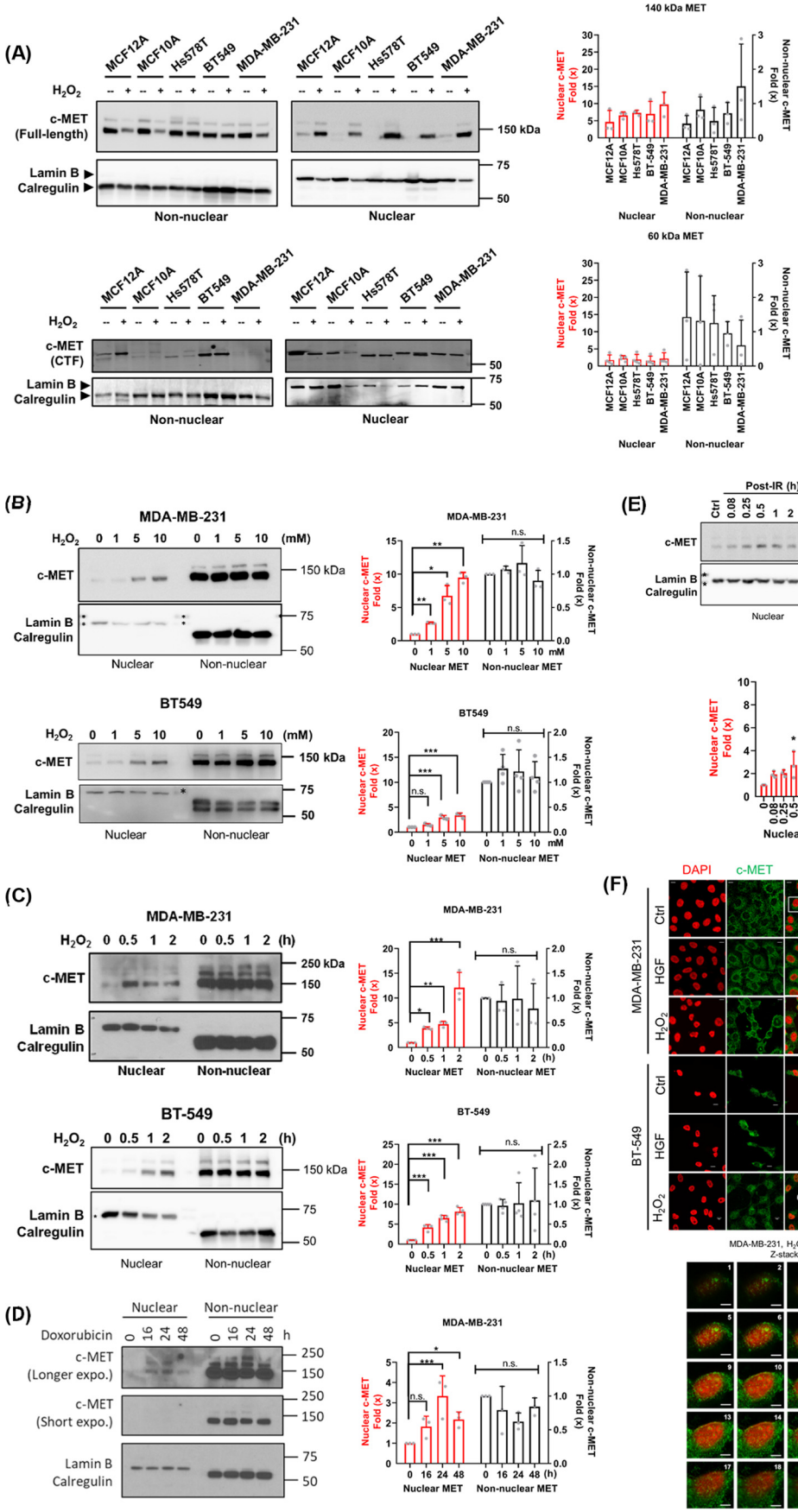

ern blotting analysis, we observed an apparent increase in the number of c-MET–containing nuclei following H_2O_2 treatment but only subtle increases in those treated with HGF (Fig. 1*F*). These results indicated that prolonged and high-concentration ligand stimulation at 100 ng/ml can induce c-MET holoreceptor nuclear translocation, but the response is less efficient than cellular stress stimulation.

Microtubules mediate full-length c-MET transport to the Golgi

As mentioned, oxidative stress elicits stronger nuclear translocation of c-MET than did ligand stimulation (Fig. 1, *B* and *F*, and Fig. S2); we further investigated the mechanisms of c-MET nuclear transport under H_2O_2 stimulation. Based on the detection of full-length c-MET, which contains the transmembrane domain, we speculated that c-MET nuclear trafficking may occur via the membrane-bound INTERNET retrograde trafficking mechanism utilized by EGFR. To validate our hypothesis, MDA-MB-231 cells were treated with Golgi apparatus inhibitor brefeldin A (BFA) for 30 min to interrupt normal Golgi function prior to H_2O_2 treatment. BFA treatment decreased the accumulation of nuclear c-MET holoreceptor (Fig. 2*A*), suggesting that c-MET is transported to the Golgi apparatus before reaching the nucleus.

Membrane-bound cargo transport requires microtubules; therefore, we investigated whether disrupting the microtubule assembly also affects c-MET nuclear transport. We found that H_2O_2-induced c-MET nuclear translocation is reduced in cells pretreated with microtubule-depolarizing agent nocodazole, as well as microtubule dynamicity-decreasing agent paclitaxel (Fig. 2, *B* and *C*). Because c-MET is primarily localized in the cytosol in breast cancer cells under normal culture condition, it may be challenging to determine whether the cytoskeleton is important for c-MET nuclear transport. To this end, we investigated the effects of microtubule inhibition in membrane c-MET transport to the cytosolic compartment in HeLa cells, in which the majority of c-MET is localized in the cell membrane under normal culture condition and is widely used to demonstrate nuclear RTK transport (41–43). This microtubule-dependent c-MET transport is not limited to breast cancer cells. Membrane c-MET decreased, whereas cytosolic c-MET increased in HeLa cells and accumulated at a similar location as *trans*-Golgi protein, GalNac T2, after HGF stimulation. This accumulation was inhibited by nocodazole pretreatment (Fig. 2*D*, *yellow spots* marked by *arrows* in *inset 2*). Nocodazole treatment also decreased the internalization of membrane c-MET into the cytosol (Fig. 2*D*), suggesting that nuclear accumulation of c-MET in HeLa cells may begin as receptor endocytosis similar to that reported for EGFR nuclear transport (43, 44, 46). However, unlike EGFR transport in HeLa cells, knocking down dynein did not affect c-MET nuclear transport in MDA-MB-231 cells (Fig. 2*E*), suggesting that the microtubule-dependent transport mechanism of nuclear c-MET may rely mainly on cargo transport proteins instead of dynein in breast cancer cells. We also found that both nocodazole and paclitaxel treatments increase population of nuclear pro-MET (Fig. 2*B* and Fig. S1), a 170-kDa partially glycosylated single-chain precursor of c-MET synthesized in ER (47, 48). These findings indicate that the nuclear localized pro-MET and c-MET may both transport from ER through retrograde mechanism.

COPI and Sec61β mediate c-MET ER-to-nucleus transport

To determine whether the transport of membrane-bound c-MET to the nucleus occurs via the retrograde trafficking mechanism through the Golgi apparatus and ER, we suppressed *cis*-Golgi–to–ER retrograde transport COPI complex vesicle by knocking down its core subunit COPG1 in MDA-MB-231 cells by shRNA targeting *COPG1* to diminish vesicle trafficking from Golgi to ER. Knocking down COPG1 significantly decreased H_2O_2-induced c-MET nuclear accumulation (Fig. 3*A*). Immunofluorescent images also showed less nuclear c-MET–containing populations after H_2O_2 treatment in COPG1 knockdown cells (Fig. 3*B*). These results indicated that COPI complex plays an important role in c-MET nuclear transport and supported our hypothesis that full-length c-MET is transported from *cis*-Golgi to ER in membrane-bound vesicles via retrograde pathway similar to transportation pathway of EGFR (16).

We then investigated the transport of c-MET from ER to nucleus by using RNAi to knockdown ER membrane protein translocator Sec61β in MDA-MB-231 cells. We found that H_2O_2-induced c-MET nuclear accumulation significantly decreased in Sec61β knockdown cells (Fig. 3, *B* and *C*). Because it has been reported that RTKs can travel from the ER into the nucleus through either the INFS (through cytosol) or INTERNET (membrane bound) pathway, we performed cellular fractionation of H_2O_2-treated MDA-MB-231 cells followed by

Figure 1. H_2O_2 and HGF can both induce nuclear accumulation of full-length c-MET in breast cell lines. *A*, cells were treated with 10 mM H_2O_2 for 30 min, and cell lysates were harvested and fractionated. Full-length c-MET and pro-MET (molecular masses, 140 and 170 kDa) and MET-CTF (molecular mass, 60 kDa) were detected by Western blotting. Nuclear envelope lamin B and ER protein calregulin were used as markers for nuclear and non-nuclear fractions, respectively. Lamin B and calregulin antibodies were mixed together and hybridized at the same time to avoid cross-contamination of the fractions. Fold changes (×) of three independent experiments are indicated in histograms as means ± S.D. *B*, MDA-MB-231 and BT-549 cells were treated with different concentration of H_2O_2 for 30 min and subjected to cellular fractionation followed by Western blotting with the indicated antibodies. Fold changes (×) of three independent experiments from MDA-MB-231 and four experiments for BT-549 are indicated in histograms as means ± S.D. *C*, MDA-MB-231 and BT-549 cells were incubated with 10 mM H_2O_2 at different times as indicated before being harvested for Western blotting analysis. Fold changes (×) of three independent experiments from MDA-MB-231 and four experiments for BT-549 are indicated in histograms as means ± S.D. *D*, MDA-MB-231 was treated with 50 nM doxorubicin for the time indicated. Lamin B and calregulin were used as markers for nuclear and non-nuclear fractions, respectively. Fold changes (x) of three independent experiments are indicated in histograms as means ± S.D. *E*, cells were treated with or without 10 Gy IR and recovered for the time indicated before because harvested and subjected to cellular fractionation followed by Western blotting analysis. Control (*Ctrl*) cells were not irradiated. Fold changes (×) of three independent experiments are indicated in histograms as means ± S.D. *F*, cells were treated with 100 ng/ml HGF (2 h for MDA-MB-231 and 6 h for BT-549) or H_2O_2 for 30 min and subjected to immunostaining with c-MET antibody (*green fluorescence*) and DAPI (pseudo-colored *red*). Images of c-MET antibody and DAPI were merged to shown the nuclear location of c-MET (*yellow*). *Insets* show enlarged views of nuclear c-MET localization. *Scale bars*, 10 μm. Z-stack images with 0.30-μm interval between each slice are presented in sequence to demonstrate c-MET localized in nucleus under H_2O_2 stimulation. *Scale bars* in Z-stack images, 5 μm. Statistical analysis was performed of the colocalization coefficient of nuclear c-MET and DAPI. Each nucleus is represented by a *dot*. Confocal image quantitation shown on the *right*. The data represent means ± S.D. ***, $p < 0.001$; *n.s.*, not significant.

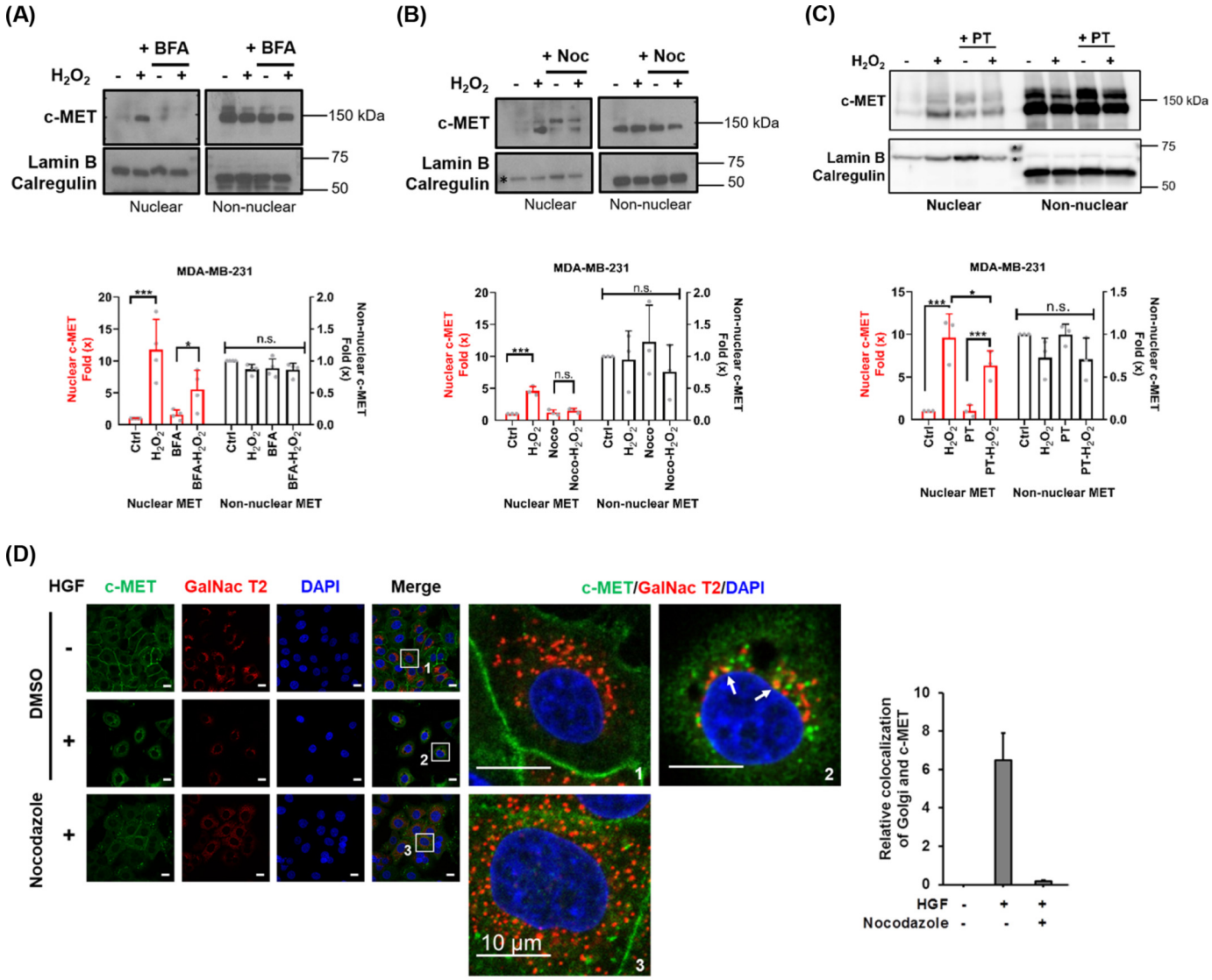

Western blotting to detect c-MET. c-MET was detected in the membrane-bound fraction but not the soluble cytosolic fraction, indicating that c-MET remains membrane-bound throughout the cytosolic trafficking process before transport into the nucleus (Fig. 3*D*). Thus, it utilizes INTERNET but not INFS pathway.

Kinase-independent transport and kinase-dependent noncanonical function of nuclear c-MET

Traditionally, RTKs are internalized from plasma membrane into the cytosol after ligand stimulation. By using c-MET autophosphorylation sites (Tyr-1234/1235) as indicators, we found H_2O_2 stimulation activated c-MET (Fig. 4*A*). Therefore, we further investigated whether this c-MET activation is required for its nuclear transport. In MDA-MB-231 and BT-549 cells, crizotinib, a c-MET kinase inhibitor inhibited H_2O_2-induced c-MET phosphorylation (Fig. 4*A*) but failed to block H_2O_2-induced c-MET nuclear accumulation (Fig. 4*B*), suggesting that nuclear transport of c-MET occurs independently of its kinase activity.

Previously, we reported that c-MET interacts with PARP1 and contributes to PARP inhibitor resistance through reduced ability of PARP1 to bind to PARP inhibitors (10). Here we showed that c-MET can also bind to KU proteins after H_2O_2 treatment, and their interactions were decreased by pretreating cells with crizotinib (Fig. 4*C*), indicating that the activated phosphorylated c-MET interacts with KU. Although PARP1 and KU are key sensors of DNA double-strand breaks (49, 50), our findings suggested that nuclear c-MET may play a role in DNA damage repair. We then investigated the effects of c-MET inhibition on DNA damage repair rate. MDA-MB-231 cells were treated with crizotinib to inhibit c-MET kinase activity and hydroxyurea and AraC to accumulate DNA damage breaks by inhibiting DNA damage repair. As shown in Fig. 4*D*, c-MET inhibition significantly delayed repair of H_2O_2-induced DNA damage based on comet assay. Together, the results suggest that c-MET may interact with KU to enhance DNA damage repair efficiency.

Discussion

H_2O_2 is an important metabolic by-product, and significant enrichment of H_2O_2 elevates cancer cell proliferation and metastasis (51). The normal physiological level of H_2O_2 is under 0.7 μM, but up to 30 mM H_2O_2 treatment will not induce cancer cell apoptosis in 6 h (52, 53), indicating that cancer cells can adapt to and survive under strong oxidative stress. In addition to H_2O_2 produced from metabolism, therapeutic agents can also induce H_2O_2 production. For example, 36-Gy IR can induce ROS at a level equivalent to 0.3 mM H_2O_2 treatment (54); 0.5 mM sodium arsenite induces similar phosphorylation of Spc1 as 1 mM H_2O_2 in cells (55), and 2 μg/ml (around 3.7 μM) doxorubicin can induce transglutaminase 2 activity at a level equivalent to 10 μM H_2O_2 (56). To date, the function of nuclear c-MET is not well-characterized in breast cancer cells because unlike the well-studied EGFR, in which EGF stimulates nuclear translocation of full-length EGFR in breast cancer cells, c-MET ligand cannot induce c-MET nuclear transport effectively (38). Moreover, it was not clear which types of cellular stress can stimulate c-MET nuclear transport. Here, we revealed that full-length c-MET nuclear accumulation is induced by elevated oxidative stresses caused by H_2O_2 and ROS-inducing anti-cancer agents in c-MET-overexpressing breast immortalized and cancer cells. Although nuclear MET-CTF has been detected in both breast and colon cancer cells by ligand induction, previous studies showed that full-length c-MET remains at plasma membrane (38, 57). Consistent with those findings, we showed that unlike ligand-stimulated nuclear EGFR accumulation, the ligand-induced nuclear accumulation of full-length c-MET can only be detected in breast cancer cells under nonphysiologically relevant high concentrations of ligand and prolonged ligand treatment (Fig. S2). These results suggested that c-MET nuclear accumulation may not be affected directly through ligand-induced activation. Although Gomes *et al.* (37) demonstrated ligand-induced full-length c-MET accumulation in hepatocyte cells and given that c-MET ligand is hepatocyte growth factor, we speculated that c-MET nuclear transport and its functions in nucleus are different in different tissues.

Nocodazole and paclitaxel can both decrease nuclear c-MET accumulation similar to EGFR, suggesting that the nuclear trafficking depends on cargo transport along microtubule. It is interesting that when we knocked down dynein, we did not observe any notable inhibition in c-MET nuclear accumulation under H_2O_2 treatment in breast cancer cell, suggesting that nuclear c-MET may utilize other cargo transporting system along microtubules. Dynein and kinesin are major microtubule cargo-transporting proteins (58). Because kinesin family is overexpressed in breast cancer and plays important roles in promoting breast cancer progression (59–61), it is conceivable, yet needs to be confirmed, that nuclear c-MET may utilize kinesin rather than dynein transport in breast cancer cells. In addition, it has been reported that cargo transport function can be rescued by activation of kinesin-14 in dynein-knockdown cells (62). We speculated that knocking down dynein triggered a

Figure 2. Nuclear accumulation of full-length c-MET can be inhibited by Golgi and microtubule disruption. *A*, MDA-MB-231 cells were treated with 5 μM BFA for 30 min prior to 30-min 10 mM H_2O_2 treatment before fractionation. Lamin B and calregulin were used as markers for nuclear and non-nuclear fractions, respectively. Fold change of MET from four independent experiments are summarized in histograms as means ± S.D. *B*, MDA-MB-231 cells were treated with nocodazole (*Noc*) for 30 min before H_2O_2 stimulation and cellular fractionation. Normalized fold change of MET from three independent experiments are shown as means ± S.D. in histograms. *C*, MDA-MB-231 cells were treated with 1 μM paclitaxel (*PT*) for 4 h before H_2O_2 stimulation and cellular fractionation. Normalized fold change of MET from three independent experiments are shown as means ± S.D. in histograms. *D*, HeLa cells were treated with solvent (DMSO), with HGF (+) or without HGF (−), and nocodazole before fixation for immunofluorescence staining for c-MET (*green*), GalNac T2 (*red*), and DAPI (*blue*). *Insets* show enlarged views of nuclear c-MET localization. *Scale bars*, 10 μm. *E*, *left panel*, knockdown of dynein by transient transfection of two different siRNAs (Dynein siRNA 1 and 2) in MDA-MB-231 cells. *Right panel*, control and dynein knockdown MDA-MB-231 cells were treated with H_2O_2 and subjected to fractionation followed by Western blotting analysis. Lamin B and calregulin were used as markers for nuclear and non-nuclear fractions, respectively. Knockdown efficiencies from four experiments are shown in histograms as means ± S.D. Fold changes (×) of three independent experiments are indicated in histograms as means ± S.D.

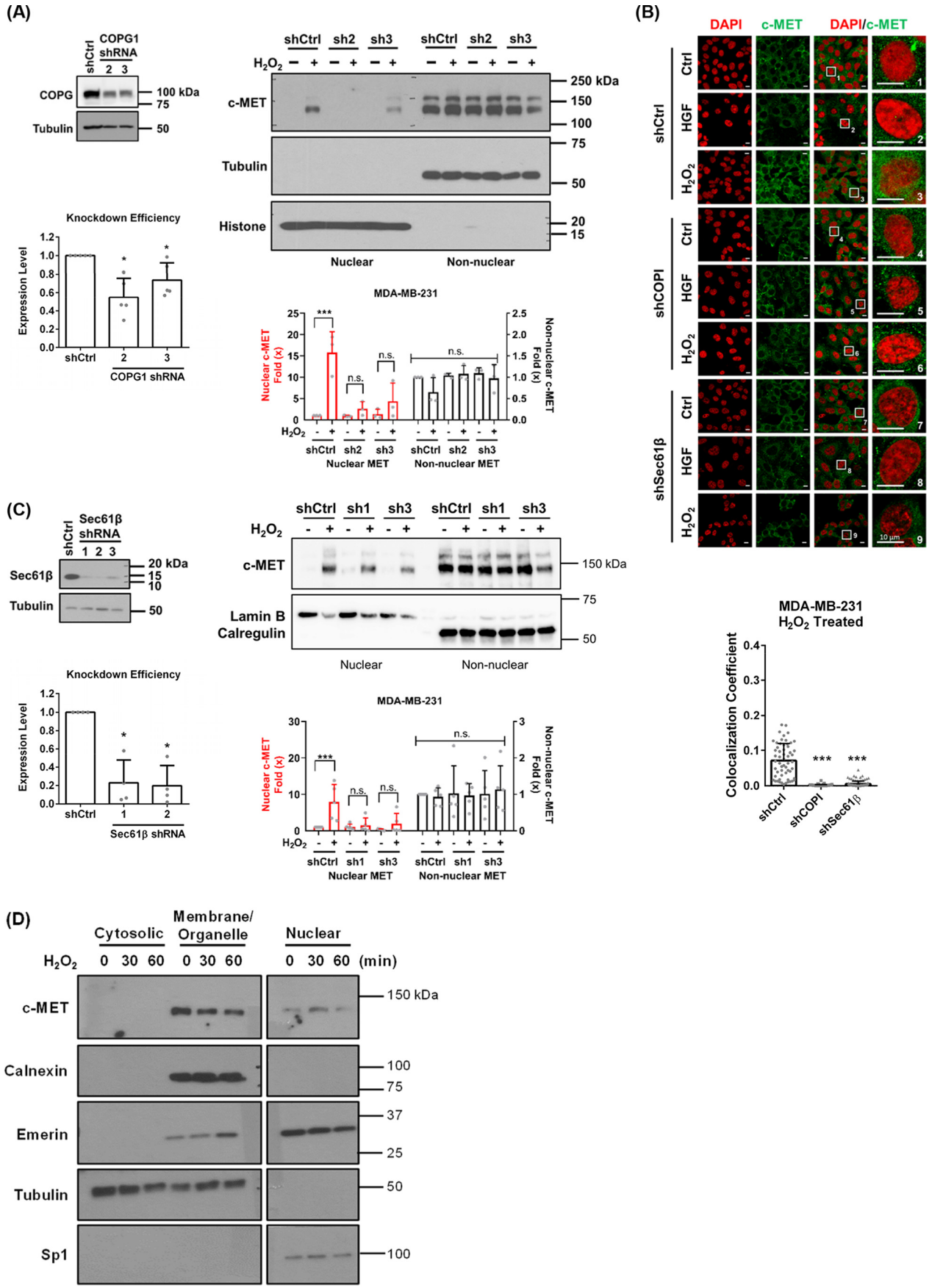

feedback regulation between dynein and kinesin and thus restored c-MET nuclear accumulation in dynein-knockdown cells. It is reported that kinesin family proteins are overexpressed in breast cancer and are related to drug resistance and poor prognosis (63, 64); we speculated that kinesin may contribute to c-MET transportation in breast cancer cells. There are 45 kinesin family genes in humans (65), it may require a systematic study to clarify whether kinesin is involved in and, if so, which kinesin may play a role in c-MET nuclear transport in breast cancer cells.

We found that c-MET nuclear accumulation induction agents include doxorubicin, arsenite, and IR, indicating the function of nuclear full-length c-MET may be closely related to resistance of anti-cancer therapeutic agents. Indeed, although we previously reported that c-MET can interact with and phosphorylate PARP1 to cause resistance to PARP inhibitors (10), we further demonstrated in this study that H_2O_2-induced nuclear c-MET also interacts with KU proteins. Although DNA-damaging sensors PARP1 and KU proteins are known to compete with each other for DNA repair pathways (49, 50, 66), it would be of interest to determine the role of nuclear c-MET in DNA damage repair pathway in the future. Based on our immunoprecipitation data (Fig. 4*C*), crizotinib decreased the interaction between c-MET and PARP1, as well as that of c-MET and KU 70. The DNA damage repair rates were slower at the early time point (30 min after H_2O_2 treatment) in response to crizotinib treatment (Fig. 4*D*). These results suggested that the interactions between c-MET, PARP1, and Ku proteins may affect DNA damage repair rates. Previous studies have shown that PARP1 and KU compete with each other and affect the choice of repair pathways (50, 66). Therefore, we speculated that c-MET is involved in the early stages of DDR when PARP1 and KU proteins play key roles in pathway choices. However, more detailed investigation would be required to determine whether the decrease in repair efficiency is attributed to the different pathways utilized for repair. Other possibilities, including the reduction in the activities of DNA damage repair proteins, cannot be ruled out based on the results of the comet assay. A more complete study would be required to derive a clearer conclusion. We also demonstrated that c-MET kinase inhibitor can block H_2O_2-induced c-MET activation but cannot block H_2O_2-induced c-MET nuclear accumulation. Given that RTKs also have kinase-independent function (67, 68), it is important to investigate the transport mechanisms of c-MET because c-MET may have kinase-independent functions in the nucleus. We specifically investigated whether c-MET and EGFR share similar nuclear transport pathways because c-MET and EGFR have been shown to function as heterodimers and contribute to each one's resistance to TKI (69, 70). Although it is still unclear whether nuclear functions of EGFR can also be induced by nuclear c-MET, there is the possibility that c-MET and EGFR can assist nuclear transport of each other through heterodimer formation. Our study revealed a mechanism of c-MET nuclear transport that is similar to that of EGFR, in which full-length c-MET is transported from plasma membrane to Golgi apparatus. This process is inhibited by BFA or by knocking down *cis*-Golgi-to-ER cargo protein complex core subunit COPG1. After reaching the ER, c-MET requires the presence of Sec61β for its accumulation in the nucleus. During Sec61β-mediated transport, c-MET remains membrane-bound because it is not detected in soluble cytosolic fraction. Therefore, we concluded that c-MET follows the INTERNET mechanism instead of INFS. In summary, because c-MET overexpression is highly correlated to poor cancer patient prognosis and the oncogenic functions of EGFR/c-MET heterodimers, in-depth studies are required in the future to explore both kinase-dependent and kinase-independent noncanonical functions of nuclear c-MET.

Experimental procedures

Materials

The antibodies used in this study are MET (C-12) antibody (sc-10; Santa Cruz Biotechnology Inc.), MET (D1C2) antibody (8198S; Cell Signaling Technology, Inc.), phospho-MET (Tyr-1234/1235) (D26) antibody (3077; Cell Signaling Technology, Inc.), lamin B1 (C-5) antibody (sc-365962; Santa Cruz Biotechnology Inc.), calregulin (H-170) antibody (sc-11398; Santa Cruz Biotechnology Inc.), COPG (H-300) antibody (sc-30092; Santa Cruz Biotechnology Inc.), Sp1 (PEP 2) antibody (sc-59; Santa Cruz Biotechnology Inc.), calnexin (C-20) antibody (sc-6465; Santa Cruz Biotechnology Inc.), Dynein 1C intermediate chain antibody (sc-13524; Santa Cruz Biotechnology Inc.), Sec61β antibody (GTX129852; GeneTex, Inc.), α-tubulin (clone B5-1-2) antibody (T5168; Sigma–Aldrich), actin antibody (A2066; Sigma–Aldrich Inc.), histone H3 antibody (ab1791; Abcam Inc.), PARP (46D11) antibody (9532; Cell Signaling Technology, Inc.), Ku80 [N3C2] antibody (GTX109935; GeneTex, Inc.), and Ku70 antibody (GTX101820; GeneTex, Inc.).

Figure 3. Full-length c-MET nuclear accumulation requires COPI- and Sec61β-mediated vesicle transport. *A*, stable knockdown of *COPGI* by two different shRNAs (shCOPG1-2 and 3) in MDA-MB-231 cells. Cells containing nontargeting scrambled shRNA were used as control (shCtrl). Knockdown efficiencies from five experiments are shown in histograms as means ± S.D. The cells were treated with 10 mM H_2O_2 for 30 min and subjected to cellular fractionation followed by Western blotting analysis. Tubulin and histone were used as markers for non-nuclear and nuclear fractions, respectively. Fold changes (×) of three independent experiments are indicated in histograms as means ± S.D. Individual values are shown as *dots*. *B*, shRNA control (shCtrl), COPG1-knockdown (shCOPI), and Sec61β-knockdown (shSec61β) MDA-MB-231 cells were treated with either 100 ng/ml HGF for 1 h or 10 mM H_2O_2 for 30 min before fixation for immunofluorescence staining. *Green*, c-MET; DAPI, nucleus. The images of c-MET and DAPI were merged to shown the intracellular location of c-MET. *Insets* show enlarged views of the nuclear region of cell. *Scale bars*, 10 μm. Statistical analysis showing the colocalization coefficient of nuclear c-MET and DAPI. Each nucleus is represented by a *dot*. Quantitation is shown on the *right*. The data represent means ± S.D. ***, $p < 0.001$. *C*, knockdown of Sec61β is stably knocked down by three different shRNAs (shSec61β-1, -2 and -3) targeting Sec61β gene in MDA-MB-231 cells. Knockdown efficiencies from four experiments are shown in histograms as means ± S.D. The cells were treated with 10 mM H_2O_2 for 30 min and subjected to cellular fractionation followed by Western blotting analysis. Tubulin and histone were used as markers for non-nuclear fraction and nuclear fractions, respectively. A statistic of five independent experiments are indicated in histograms as means ± S.D. Individual values are shown as *dots*. *D*, MDA-MB-231 cells were treated with 10 mM H_2O_2 and subjected to cellular fractionation using ProteoExtract® subcellular proteome extraction kit. Tubulin and Sp1 was used as markers for non-nuclear and nuclear fractions, respectively. Calnexin was used as marker for membrane-bound non-nuclear fraction. Emerin is a protein predominantly located in the Golgi and nuclear membrane and is used as a marker for membrane-bound organelles, including the nucleus.

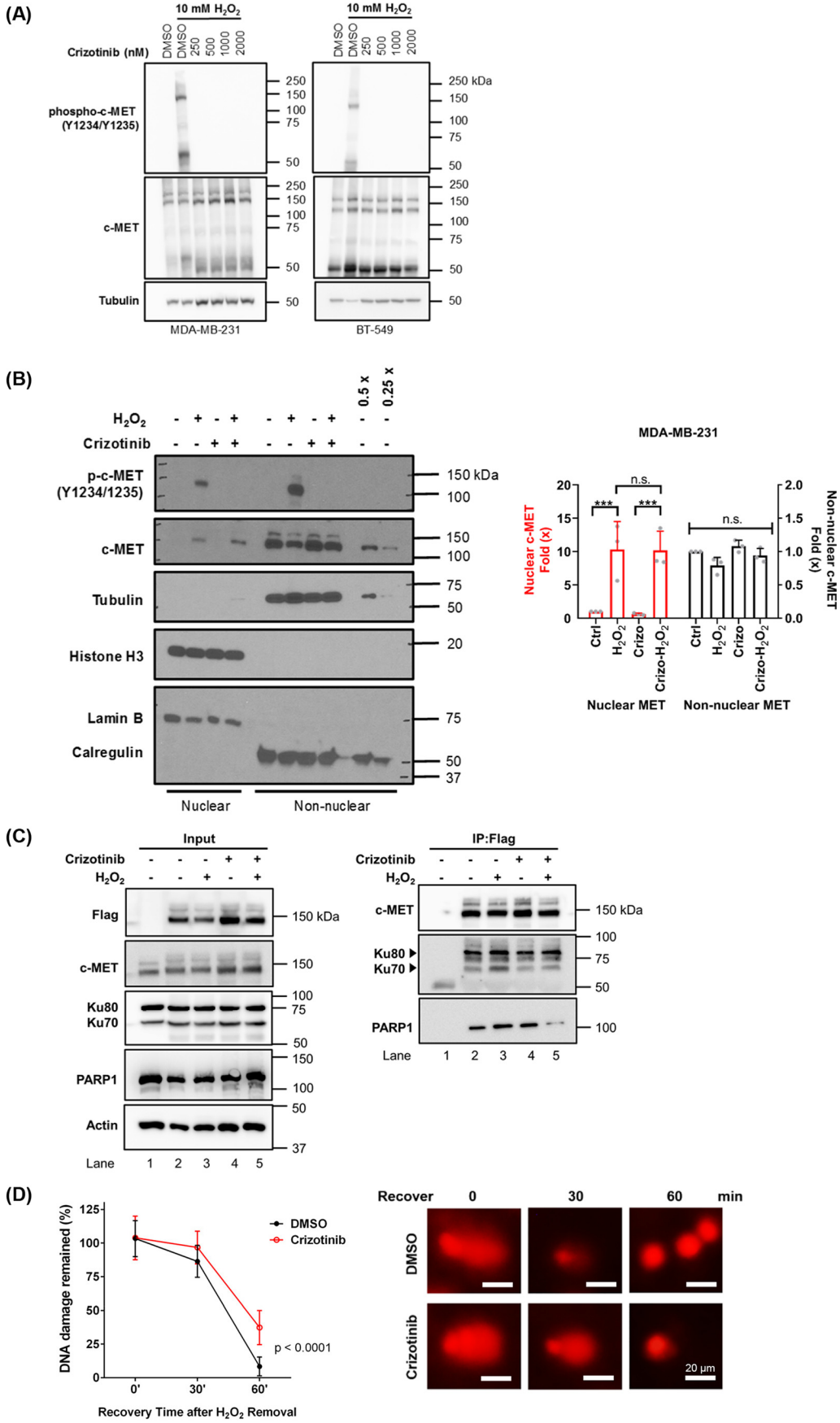

HGF human recombinant was purchased from BioVision Inc. H_2O_2, BFA, nocodazole, and paclitaxel were purchased from Sigma–Aldrich.

Cell culture

All cell lines were originally obtained from ATCC (Manassas, VA). MDA-MB-231, BT549, and Hs578T cells were maintained in Dulbecco's modified Eagle's medium (DMEM)/F12 with 10% fetal bovine serum in the presence of 100 units/ml penicillin and 100 μg/ml streptomycin. MCF-10A and MCF-12A cells were maintained in DMEM/F12 medium with 5% horse serum in the presence of 100 units/ml penicillin, 100 μg/ml streptomycin, 10 μg/ml insulin, 20 ng/ml EGF, 100 ng/ml cholera enterotoxin, 0.5 μg/ml hydrocortisone, and 1 mM calcium chloride. Cell lines were validated by STR DNA fingerprinting using the AmpF_STR Identifiler kit according to manufacturer's instructions (Applied Biosystems catalog no. 4322288). The STR profiles were compared with known ATCC fingerprints and to the Cell Line Integrated Molecular Authentication database version 0.1.200808 (http://bioinformatics.hsanmartino.it/clima/) (71).[3] The STR profiles matched known DNA fingerprints.

The cells were incubated in serum-depleted medium for 18 h before HGF treatment but not before H_2O_2 treatment. The cells were treated with 100 ng/ml HGF or 10 mM H_2O_2 in the culture medium and incubated at 37 °C water-saturated incubator supplied with 5% CO_2 for the times indicated. 50 mM H_2O_2 is freshly prepared by adding 30% H_2O_2 stock into cell culture medium in a ratio of 5.75 μl/ml. The 50 mM H_2O_2 were then further diluted to working concentration with cell culture medium.

Cell fractionation

Nuclear and non-nuclear cell fractionations were performed as previously described (43). Briefly, cells were harvested at 90% confluency and lysed in Nori lysis buffer (20 mM HEPES, pH 7.0, 10 mM KCl, 0.5% Nonidet P-40, 2 mM $MgCl_2$, 2 mM Na_3VO_4, 1 mM phenylmethylsulfonyl fluoride, and 0.15 mg/ml aprotinin) on ice for at least 10 min. Following lysis, the cells were homogenized by Dounce homogenizer and centrifuged 1,500 × *g* for 5 min, and the supernatants were collected as non-nuclear fractions. The pelleted nuclei were washed with the same lysis buffer and centrifuged 1,500 × *g* for 5 min to sediment nuclear pellet. The pellets were then solubilized in NETN buffer (150 mM NaCl, 1 mM EDTA, 20 mM Tris-Cl, pH 8.0, 0.5% Nonidet P-40, and protease inhibitor mixture mixture) and incubated on ice for 10 min before 10-s sonication three times (Sonics Vibra-Cell, amplitude 30; Sonics & Materials, Newtown, CT). The extract was centrifuged at maximum speed for 10 min. The supernatant was collected as nuclear fraction. The soluble cytosolic and membrane cell fractionations were performed by using ProteoExtract® subcellular proteome extraction kit (Calbiochem® Merck Millipore) following the manufacturer's protocol with modifications as described (18).

Western blotting analysis

For detecting proteins in cell fractionation samples, 40–60 μg of proteins were loaded for each lane in SDS-PAGE. The same amounts of nuclear and non-nuclear fraction proteins were used in Western blotting analysis. Primary antibodies were hybridized at 4 °C overnight and followed by horseradish peroxidase-conjugated secondary antibody hybridization. The images were quantified by using Image Studio™ Lite version 5.2.

For cellular fractionation experiments, nuclear envelope protein lamin B or histone H3 was used to indicate the cell nuclear fraction. Both proteins were used to insure that H_2O_2 treatment does not cause protein degradation in either of the proteins. ER protein calregulin was used to indicate that there is no contamination of ER proteins in nuclear fraction. Tubulin was used to signify non-nuclear fractionation.

Immunoprecipitation

Immunoprecipitation is performed with MDA-MB-231 cells or MDA-MB-231 cell that stably expressing FLAG-tagged c-MET. Indicated in the experiment, the cells were incubated with or without 500 nM crizotinib overnight before stimulated with 10 mM H_2O_2 for 30 min prior to lysate collection. In brief, the cells were lysed in radioimmune precipitation assay buffer (150 mM NaCl, 1% Triton X-100, 0.1% SDS, 50 mM Tris-HCl, pH 7.5, and protease inhibitor cacktail), and 500 μg of total protein was used for immunoprecipitation by incubating with anti-FLAG® M2 affinity gel beads (Sigma–Aldrich) overnight rotating at 4 °C. Precipitates were washed three times with immunoprecipitation wash buffer (20 mM Tris, pH 7.5, 150 mM NaCl, 1 mM EDTA, 1 mM EGTA, 1% Triton X-100, 2.5 mM sodium pyrophosphate, 1 mM β-glycerophosphate, 1 mM Na_3VO_4, 1 μg/ml leupeptin) and eluted from magnetic beads using SDS-PAGE sample buffer.

[3] Please note that the JBC is not responsible for the long-term archiving and maintenance of this site or any other third party hosted site.

Figure 4. Inhibiting c-MET kinase activity diminishes interaction of c-MET and DNA repair proteins without affecting nuclear accumulation. *A*, analysis of c-MET inhibitor on H_2O_2-induced c-MET tyrosine (*Y*) 1234 and 1235 phosphorylation. The cells were treated with crizotinib overnight at various concentrations indicated followed by 30-min H_2O_2 treatment. The cells were then harvested, and whole cell lysates were used for Western blotting analysis. *B*, cells were treated with (+) or without (−) crizotinib overnight followed by 30-min H_2O_2 treatment and cellular fractionation. Different amounts of non-nuclear fractionated proteins from solvent-treated group were used to estimate the amount of c-MET in the nucleus. *0.5*×, half amount of protein was loaded; *0.25*×, a quarter amount of protein loaded. Lamin B and histone were used as markers for nuclear fractions, and calregulin and tubulin were used for non-nuclear fractions. *C*, MDA-MB-231 (*lane 1*) and MDA-MB-231 cells overexpressing FLAG-tagged c-MET (*lanes 2–4*) were treated with crizotinib and H_2O_2 alone or in combination. c-MET was then immunoprecipitated (*IP*) by using FLAG-tag antibody, and the precipitates were subjected to Western blotting analysis with PARP1, Ku70, Ku80, and actin antibodies. Inputs were cell lysates prior to immunoprecipitation. *D*, MDA-MB-231 cells were treated with hydroxyurea/AraC to inhibit DNA damage repair for overnight followed by 30-min 10 mM H_2O_2 treatment. The H_2O_2- and hydroxyurea/AraC– containing media were then removed, and the cells were released for DNA damage repair in fresh culture media. The cells were then collected for comet assay analysis at different time points after release (recovery time). The amounts of DNA fragments in comet tail (% DNA in tail) were used as a parameter to calculate DNA damage. DNA damage was normalized to that in in the untreated group (0 min) as 100%. The data represent the means ± S.D. ($p < 0.0001$, two-way analysis of variance). Representative images of the comet assay are shown. *Scale bars*, 20 μm. DNA was stained with propidium iodide and imaged under fluorescence microscope. *n.s.*, not significant.

Table 1
RNAi sequences targeting COPG1 and Sec61β
CDS, coding DNA sequence.

	Target	Oligo/clone ID	Sequences
shRNA			
shCOPG1-2	NM_016128 CDS	TRCN0000148567	CCGGCCTAGCCGTCAATAAGATGATCTCGAGATCATCTTATTGACGGCTAGGTTTTTTG
shCOPG1-3	NM_016128 3′-UTR	TRCN0000149699	CCGGGCTTGTCCTAAATCTTGCTGTCTCGAGACAGCAAGATTTAGGACAAGCTTTTTTG
shSec61β-1	NM_006808 3′-UTR	TRCN0000179927	CCGGCCCAACATTTCTTGGACCAAACTCGAGTTTGGTCCAAGAAATGTTGGGTTTTTTG
shSec61β-2	NM_006808 3′-UTR	TRCN0000183459	CCGGGTATAGTGACTATCTGTTCATCTCGAGATGAACAGATAGTCACTATACTTTTTG
shSec61β-3	NM_006808 CDS	TRCN0000147459	CCGGCAGTATTGGTTATGAGTCTTCCTCGAGGAAGACTCATAACCAATACTGTTTTTTG
siRNA			
siDyn1	DYNC1I1	SASI_Hs02_00337554; SASI_Hs01_00052798; SASI_Hs01_00052802	
siDyn2	DYNC1I2	SASI_Hs01_00129736; SASI_Hs01_00129737; SASI_Hs02_00331729	

RNA interference

COPG1 or Sec61β knockdown MDA-MB-231 stable clones were established via lentiviral gene delivery. The lentivirus particles are produced by transfecting HEK293T cells with pCMV-VSVG, pCMV-Δ 8.91, and shRNA plasmid in a ratio of 5:1:10. Transfectants were selected by using 1% puromycin-containing DMEM/F12 medium, and stable transfectants were maintained with 0.5% puromycin-containing DMEM/F12 selective medium. The shRNA expression vectors with pLKO.1 backbone was purchased from Sigma–Aldrich, and the sequences are shown in Table 1. Scrambled shRNA (addgene plasmid 1864) was used as nontargeting shRNA controls (shCtrl) for these experiments (45). Dynein intermediate chain transient knockdown were performed with siRNA purchased from Sigma–Aldrich (Table 1). 90 nM siRNA were mixed with Lipofectamine 3000 reagent (Thermo Fisher Scientific) in Opti-MEM medium (Gibco, Thermo Fisher Scientific). The cells were H_2O_2 treated and harvested for fractionation experiments 3 days after transfection.

Confocal microscopy

Samples for confocal microscopy were prepared as described previously (16). In brief, the cells were seeded on chamber slides for at least 18 h before treatment. After treatment, the cells were washed with PBS, fixed with 4% paraformaldehyde, permeablized with 0.25% Triton X-100/PBS, and stained with the indicated primary or fluorescent-labeled secondary antibodies. Primary antibodies were diluted in 3% normal goat serum/PBST at the following ratios: c-MET (C-12) antibody, 1:100, HGF antibody, 1:100, and GalNac T2, 1:100. DNA was counterstained with DAPI-containing mounting solution (Vector Laboratories Inc.). Immunostained cells were examined and imaged with Zeiss LSM 710 laser microscope.

Comet assay

After DNA damage induced by H_2O_2 treatment, cell culture medium was refreshed to allow DNA damage repair process. The base layer of comet slides was prepared with 1.4% high melting temperature agarose and solidified on ice. The cells were harvested at the times indicated, mixed with 1.2% low melting temperature agarose at 1:1 (v/v) ratio, and put onto the base layer of comet slides. The slides were then covered with 1.2% low melting agarose gel and incubated overnight in lysis buffer (2.5 M NaCl, 100 mM EDTA, 10 mM Tris, pH 10, 1% *N*-laurylsarcosine, 1% Triton, and 10% DMSO). The slides were washed in di-deionized water five times before DNA were denatured in alkaline comet electrophoresis buffer (0.3 N NaOH, 1 mM EDTA) for 25 min. Electrophoresis was performed with alkaline comet electrophoresis buffer at 0.3 A, 25 V for 25 min. Each slide was washed with di-deionized water and transferred to 0.4 M Tris-Cl (pH 7.5) until DNA was stained by applying 40 μl of propidium iodide (50 μg/ml) onto the slides. A coverslip was applied, and the slides were subjected to examination with fluorescence microscope (Zeiss). Images of at least 50 cells/treatment were recorded with close-circuit display camera (CoolSNAP). DNA damage is quantified by using CometScore (tritekcorp) with a percentages of DNA in tail parameter.

Statistical analysis

For Western blotting signal quantifications, signal intensities were analyzed by using Image Studio Lite (version 5.2) (LI-COR Biosciences, Lincoln, NE). MET signal intensities were first normalized to that of loading control proteins such as lamin B or calregulin before the signals from treatment groups were normalized again to the control group in the experiments. Unless specified, 140-kDa mature MET signal is quantified in Western blotting. Every independent experiment repeats was quantified individually. Fold changes (×) in Western blotting signals were analyzed by a nonparametric Friedman test using the GraphPad Prism 8.0 software. The percentage of MET-containing cell nuclei was calculated based on the immunofluorescent images obtained by confocal microscopy, and at least 160 cell nuclei were counted for each experiment. The differences in colocalization coefficient were analyzed by a nonparametric Kruskal–Wallis test using the GraphPad Prism 8.0 software. A p value less of 0.05 was considered statistically significant (*, $p < 0.05$; **, $p < 0.002$; ***, $p < 0.001$).

Author contributions—M.-K. C. and Y. D. conceptualization; M.-K. C., Y. D., L. S., Y.-H. W., Y. G., and J. H. data curation; M.-K. C. formal analysis; M.-K. C. investigation; M.-K. C. methodology; M.-K. C. writing-original draft; Y. D. validation; J. L. H. and M.-C. H. writing-review and editing; M.-C. H. resources; M.-C. H. supervision; M.-C. H. funding acquisition; M.-C. H. project administration.

Acknowledgment—STR DNA fingerprinting was done by the Cancer Center Support Grant-funded Characterized Cell Line core under Grant NCI CA016672.

References

1. Gorrini, C., Harris, I. S., and Mak, T. W. (2013) Modulation of oxidative stress as an anticancer strategy. *Nat. Rev. Drug. Discov.* **12,** 931–947 CrossRef Medline
2. Sies, H. (2017) Hydrogen peroxide as a central redox signaling molecule in physiological oxidative stress: oxidative eustress. *Redox. Biol.* **11,** 613–619 CrossRef Medline
3. Galadari, S., Rahman, A., Pallichankandy, S., and Thayyullathil, F. (2017) Reactive oxygen species and cancer paradox: to promote or to suppress? *Free Radic. Biol. Med.* **104,** 144–164 CrossRef Medline
4. Di Meo, S., Reed, T. T., Venditti, P., and Victor, V. M. (2016) Role of ROS and RNS sources in physiological and pathological conditions. *Oxid. Med. Cell Longev.* **2016,** 1245049 Medline
5. Yang, W., Zou, L., Huang, C., and Lei, Y. (2014) Redox regulation of cancer metastasis: molecular signaling and therapeutic opportunities. *Drug Dev. Res.* **75,** 331–341 CrossRef Medline
6. Bae, Y. S., Kang, S. W., Seo, M. S., Baines, I. C., Tekle, E., Chock, P. B., and Rhee, S. G. (1997) Epidermal growth factor (EGF)-induced generation of hydrogen peroxide: role in EGF receptor-mediated tyrosine phosphorylation. *J. Biol. Chem.* **272,** 217–221 CrossRef Medline
7. Lo, H. W., and Hung, M. C. (2006) Nuclear EGFR signalling network in cancers: linking EGFR pathway to cell cycle progression, nitric oxide pathway and patient survival. *Br. J. Cancer* **94,** 184–188 CrossRef Medline
8. Kodiha, M., and Stochaj, U. (2012) Nuclear transport: a switch for the oxidative stress-signaling circuit? *J. Signal Transduct.* **2012,** 208650 Medline
9. Dittmann, K., Mayer, C., Kehlbach, R., Rothmund, M. C., and Peter Rodemann, H. (2009) Radiation-induced lipid peroxidation activates src kinase and triggers nuclear EGFR transport. *Radiother. Oncol.* **92,** 379–382 CrossRef Medline
10. Du, Y., Yamaguchi, H., Wei, Y., Hsu, J. L., Wang, H. L., Hsu, Y. H., Lin, W. C., Yu, W. H., Leonard, P. G., Lee, G. R., 4th, Chen, M. K., Nakai, K., Hsu, M. C., Chen, C. T., Sun, Y., *et al.* (2016) Blocking c-Met-mediated PARP1 phosphorylation enhances anti-tumor effects of PARP inhibitors. *Nat. Med.* **22,** 194–201 CrossRef Medline
11. Wang, S. C., and Hung, M. C. (2009) Nuclear translocation of the epidermal growth factor receptor family membrane tyrosine kinase receptors. *Clin. Cancer Res.* **15,** 6484–6489 CrossRef Medline
12. Chen, M. K., and Hung, M. C. (2015) Proteolytic cleavage, trafficking, and functions of nuclear receptor tyrosine kinases. *FEBS J.* **282,** 3693–3721 CrossRef Medline
13. Lee, H. H., Wang, Y. N., and Hung, M. C. (2015) Non-canonical signaling mode of the epidermal growth factor receptor family. *Am. J. Cancer Res.* **5,** 2944–2958 Medline
14. Pellett, P. A., Dietrich, F., Bewersdorf, J., Rothman, J. E., and Lavieu, G. (2013) Inter-Golgi transport mediated by COPI-containing vesicles carrying small cargoes. *Elife* **2,** e01296 CrossRef Medline
15. Spang, A. (2013) Retrograde traffic from the Golgi to the endoplasmic reticulum. *Cold Spring Harb. Perspect. Biol.* **5,** a013391 Medline
16. Wang, Y. N., Wang, H., Yamaguchi, H., Lee, H. J., Lee, H. H., and Hung, M. C. (2010) COPI-mediated retrograde trafficking from the Golgi to the ER regulates EGFR nuclear transport. *Biochem. Biophys. Res. Commun.* **399,** 498–504 CrossRef Medline
17. Liao, H. J., and Carpenter, G. (2007) Role of the Sec61 translocon in EGF receptor trafficking to the nucleus and gene expression. *Mol. Biol. Cell* **18,** 1064–1072 CrossRef Medline
18. Wang, Y. N., Lee, H. H., Lee, H. J., Du, Y., Yamaguchi, H., and Hung, M. C. (2012) Membrane-bound trafficking regulates nuclear transport of integral epidermal growth factor receptor (EGFR) and ErbB-2. *J. Biol. Chem.* **287,** 16869–16879 CrossRef Medline
19. Myers, J. M., Martins, G. G., Ostrowski, J., and Stachowiak, M. K. (2003) Nuclear trafficking of FGFR1: a role for the transmembrane domain. *J. Cell Biochem.* **88,** 1273–1291 CrossRef Medline
20. Wang, Y. N., and Hung, M. C. (2012) Nuclear functions and subcellular trafficking mechanisms of the epidermal growth factor receptor family. *Cell Biosci.* **2,** 13 CrossRef Medline
21. Lin, S. Y., Makino, K., Xia, W., Matin, A., Wen, Y., Kwong, K. Y., Bourguignon, L., and Hung, M. C. (2001) Nuclear localization of EGF receptor and its potential new role as a transcription factor. *Nat. Cell Biol.* **3,** 802–808 CrossRef Medline
22. Chen, M. K., and Hung, M. C. (2016) Regulation of therapeutic resistance in cancers by receptor tyrosine kinases. *Am. J. Cancer Res.* **6,** 827–842 Medline
23. Lo, H. W., Hsu, S. C., Ali-Seyed, M., Gunduz, M., Xia, W., Wei, Y., Bartholomeusz, G., Shih, J. Y., and Hung, M. C. (2005) Nuclear interaction of EGFR and STAT3 in the activation of the iNOS/NO pathway. *Cancer Cell* **7,** 575–589 CrossRef Medline
24. Wang, S. C., Nakajima, Y., Yu, Y. L., Xia, W., Chen, C. T., Yang, C. C., McIntush, E. W., Li, L. Y., Hawke, D. H., Kobayashi, R., and Hung, M. C. (2006) Tyrosine phosphorylation controls PCNA function through protein stability. *Nat. Cell Biol.* **8,** 1359–1368 CrossRef Medline
25. Wang, S. C., Lien, H. C., Xia, W., Chen, I. F., Lo, H. W., Wang, Z., Ali-Seyed, M., Lee, D. F., Bartholomeusz, G., Ou-Yang, F., Giri, D. K., and Hung, M. C. (2004) Binding at and transactivation of the COX-2 promoter by nuclear tyrosine kinase receptor ErbB-2. *Cancer Cell* **6,** 251–261 CrossRef Medline
26. Das, A. K., Chen, B. P., Story, M. D., Sato, M., Minna, J. D., Chen, D. J., and Nirodi, C. S. (2007) Somatic mutations in the tyrosine kinase domain of epidermal growth factor receptor (EGFR) abrogate EGFR-mediated radioprotection in non-small cell lung carcinoma. *Cancer Res.* **67,** 5267–5274 CrossRef Medline
27. Guo, G., Narayan, R. N., Horton, L., Patel, T. R., and Habib, A. A. (2017) The role of EGFR-Met interactions in the pathogenesis of glioblastoma and resistance to treatment. *Curr. Cancer Drug Targets* **17,** 297–302 CrossRef Medline
28. Gelsomino, F., Facchinetti, F., Haspinger, E. R., Garassino, M. C., Trusolino, L., De Braud, F., and Tiseo, M. (2014) Targeting the MET gene for the treatment of non-small-cell lung cancer. *Crit. Rev. Oncol. Hematol.* **89,** 284–299 CrossRef Medline
29. Shattuck, D. L., Miller, J. K., Carraway, K. L., 3rd, and Sweeney, C. (2008) Met receptor contributes to trastuzumab resistance of Her2-overexpressing breast cancer cells. *Cancer Res.* **68,** 1471–1477 CrossRef Medline
30. Troiani, T., Martinelli, E., Napolitano, S., Vitagliano, D., Ciuffreda, L. P., Costantino, S., Morgillo, F., Capasso, A., Sforza, V., Nappi, A., De Palma, R., D'Aiuto, E., Berrino, L., Bianco, R., and Ciardiello, F. (2013) Increased TGF-α as a mechanism of acquired resistance to the anti-EGFR inhibitor cetuximab through EGFR–MET interaction and activation of MET signaling in colon cancer cells. *Clin. Cancer Res.* **19,** 6751–6765 CrossRef Medline
31. Bradley, C. A., Salto-Tellez, M., Laurent-Puig, P., Bardelli, A., Rolfo, C., Tabernero, J., Khawaja, H. A., Lawler, M., Johnston, P. G., Van Schaeybroeck, S., and MErCuRIC Consortium (2017) Targeting c-MET in gastrointestinal tumours: rationale, opportunities and challenges. *Nat. Rev. Clin. Oncol.* **14,** 562–576 CrossRef Medline
32. Raghav, K. P., Wang, W., Liu, S., Chavez-MacGregor, M., Meng, X., Hortobagyi, G. N., Mills, G. B., Meric-Bernstam, F., Blumenschein, G. R., Jr., and Gonzalez-Angulo, A. M. (2012) cMET and phospho-cMET protein levels in breast cancers and survival outcomes. *Clin. Cancer Res.* **18,** 2269–2277 CrossRef Medline
33. Zagouri, F., Bago-Horvath, Z., Rössler, F., Brandstetter, A., Bartsch, R., Papadimitriou, C. A., Dimitrakakis, C., Tsigginou, A., Papaspyrou, I., Giannos, A., Dimopoulos, M. A., and Filipits, M. (2013) High MET expression is an adverse prognostic factor in patients with triple-negative breast cancer. *Br. J. Cancer* **108,** 1100–1105 CrossRef Medline
34. Inanc, M., Ozkan, M., Karaca, H., Berk, V., Bozkurt, O., Duran, A. O., Ozaslan, E., Akgun, H., Tekelioglu, F., and Elmali, F. (2014) Cytokeratin 5/6, c-Met expressions, and PTEN loss prognostic indicators in triple-negative breast cancer. *Med. Oncol.* **31,** 801 CrossRef Medline
35. Hsu, Y. H., Yao, J., Chan, L. C., Wu, T. J., Hsu, J. L., Fang, Y. F., Wei, Y., Wu, Y., Huang, W. C., Liu, C. L., Chang, Y. C., Wang, M. Y., Li, C. W., Shen, J., Chen, M. K., *et al.* (2014) Definition of PKC-α, CDK6, and MET as therapeutic targets in triple-negative breast cancer. *Cancer Res.* **74,** 4822–4835 CrossRef Medline

36. Zhao, S., Cao, L., and Freeman, J. W. (2013) Knockdown of RON receptor kinase delays but does not prevent tumor progression while enhancing HGF/MET signaling in pancreatic cancer cell lines. *Oncogenesis* **2,** e76 CrossRef Medline
37. Gomes, D. A., Rodrigues, M. A., Leite, M. F., Gomez, M. V., Varnai, P., Balla, T., Bennett, A. M., and Nathanson, M. H. (2008) c-Met must translocate to the nucleus to initiate calcium signals. *J. Biol. Chem.* **283,** 4344–4351 CrossRef Medline
38. Matteucci, E., Bendinelli, P., and Desiderio, M. A. (2009) Nuclear localization of active HGF receptor Met in aggressive MDA-MB231 breast carcinoma cells. *Carcinogenesis* **30,** 937–945 CrossRef Medline
39. Shimizu, S., Ishii, M., Yamamoto, T., and Momose, K. (1997) Mechanism of nitric oxide production induced by H_2O_2 in cultured endothelial cells. *Res. Commun. Mol. Pathol. Pharmacol.* **95,** 227–239 Medline
40. Björkman, U., and Ekholm, R. (1995) Hydrogen peroxide degradation and glutathione peroxidase activity in cultures of thyroid cells. *Mol. Cell Endocrinol.* **111,** 99–107 CrossRef Medline
41. Yuan, Y., Chen, S., Paunesku, T., Gleber, S. C., Liu, W. C., Doty, C. B., Mak, R., Deng, J., Jin, Q., Lai, B., Brister, K., Flachenecker, C., Jacobsen, C., Vogt, S., *et al.* (2013) Epidermal growth factor receptor targeted nuclear delivery and high-resolution whole cell X-ray imaging of Fe3O4@TiO2 nanoparticles in cancer cells. *ACS Nano* **7,** 10502–10517 CrossRef Medline
42. Wei, H., Zhu, Z., and Lu, L. (2017) Inhibition of EGFR nuclear shuttling decreases irradiation resistance in HeLa cells. *Folia Histochem. Cytobiol.* **55,** 43–51 CrossRef Medline
43. Du, Y., Shen, J., Hsu, J. L., Han, Z., Hsu, M. C., Yang, C. C., Kuo, H. P., Wang, Y. N., Yamaguchi, H., Miller, S. A., and Hung, M. C. (2014) Syntaxin 6–mediated Golgi translocation plays an important role in nuclear functions of EGFR through microtubule-dependent trafficking. *Oncogene* **33,** 756–770 Medline
44. Li, H., Duan, Z. W., Xie, P., Liu, Y. R., Wang, W. C., Dou, S. X., and Wang, P. Y. (2012) Effects of paclitaxel on EGFR endocytic trafficking revealed using quantum dot tracking in single cells. *PLoS One* **7,** e45465 CrossRef Medline
45. Sarbassov, D. D., Guertin, D. A., Ali, S. M., and Sabatini, D. M. (2005) Phosphorylation and regulation of Akt/PKB by the rictor-mTOR complex. *Science* **307,** 1098–1101 CrossRef Medline
46. Lo, H. W., Ali-Seyed, M., Wu, Y., Bartholomeusz, G., Hsu, S. C., and Hung, M. C. (2006) Nuclear-cytoplasmic transport of EGFR involves receptor endocytosis, importin β1 and CRM1. *J. Cell Biochem.* **98,** 1570–1583 CrossRef Medline
47. Chen, R., Li, J., Feng, C. H., Chen, S. K., Liu, Y. P., Duan, C. Y., Li, H., Xia, X. M., He, T., Wei, M., and Dai, R. Y. (2013) c-Met function requires *N*-linked glycosylation modification of pro-Met. *J. Cell Biochem.* **114,** 816–822 CrossRef Medline
48. Giordano, S., Di Renzo, M. F., Narsimhan, R. P., Cooper, C. S., Rosa, C., and Comoglio, P. M. (1989) Biosynthesis of the protein encoded by the c-met proto-oncogene. *Oncogene* **4,** 1383–1388 Medline
49. Yang, G., Liu, C., Chen, S. H., Kassab, M. A., Hoff, J. D., Walter, N. G., and Yu, X. (2018) Super-resolution imaging identifies PARP1 and the Ku complex acting as DNA double-strand break sensors. *Nucleic Acids Res.* **46,** 3446–3457 CrossRef Medline
50. Wang, M., Wu, W., Wu, W., Rosidi, B., Zhang, L., Wang, H., and Iliakis, G. (2006) PARP-1 and Ku compete for repair of DNA double strand breaks by distinct NHEJ pathways. *Nucleic Acids Res.* **34,** 6170–6182 CrossRef Medline
51. Lisanti, M. P., Martinez-Outschoorn, U. E., Lin, Z., Pavlides, S., Whitaker-Menezes, D., Pestell, R. G., Howell, A., and Sotgia, F. (2011) Hydrogen peroxide fuels aging, inflammation, cancer metabolism and metastasis: the seed and soil also needs "fertilizer." *Cell Cycle* **10,** 2440–2449 Medline
52. Weinstain, R., Savariar, E. N., Felsen, C. N., and Tsien, R. Y. (2014) *In vivo* targeting of hydrogen peroxide by activatable cell-penetrating peptides. *J. Am. Chem. Soc.* **136,** 874–877 CrossRef Medline
53. Habold, C., Poehlmann, A., Bajbouj, K., Hartig, R., Korkmaz, K. S., Roessner, A., and Schneider-Stock, R. (2008) Trichostatin A causes p53 to switch oxidative-damaged colorectal cancer cells from cell cycle arrest into apoptosis. *J. Cell Mol. Med.* **12,** 607–621 CrossRef Medline
54. Dahm-Daphi, J., Sass, C., and Alberti, W. (2000) Comparison of biological effects of DNA damage induced by ionizing radiation and hydrogen peroxide in CHO cells. *Int. J. Radiat. Biol.* **76,** 67–75 CrossRef Medline
55. Rodríguez-Gabriel, M. A., and Russell, P. (2005) Distinct signaling pathways respond to arsenite and reactive oxygen species in *Schizosaccharomyces pombe*. *Eukaryot. Cell* **4,** 1396–1402 CrossRef Medline
56. Han, J. A., and Park, S. C. (1999) Hydrogen peroxide mediates doxorubicin-induced transglutaminase 2 expression in PC-14 human lung cancer cell line. *Exp. Mol. Med.* **31,** 83–88 CrossRef Medline
57. Pozner-Moulis, S., Pappas, D. J., and Rimm, D. L. (2006) Met, the hepatocyte growth factor receptor, localizes to the nucleus in cells at low density. *Cancer Res.* **66,** 7976–7982 CrossRef Medline
58. Hagiwara, H., Yorifuji, H., Sato-Yoshitake, R., and Hirokawa, N. (1994) Competition between motor molecules (kinesin and cytoplasmic dynein) and fibrous microtubule-associated proteins in binding to microtubules. *J. Biol. Chem.* **269,** 3581–3589 Medline
59. Telikicherla, D., Maharudraiah, J., Pawar, H., Marimuthu, A., Kashyap, M. K., Ramachandra, Y. L., Roa, J. C., and Pandey, A. (2012) Overexpression of kinesin associated protein 3 (KIFAP3) in breast cancer. *J. Proteomics Bioinform.* **5,** 122–126 Medline
60. Wang, Q., Zhao, Z. B., Wang, G., Hui, Z., Wang, M. H., Pan, J. F., and Zheng, H. (2013) High expression of KIF26B in breast cancer associates with poor prognosis. *PLoS One* **8,** e61640 CrossRef Medline
61. Groth-Pedersen, L., Aits, S., Corcelle-Termeau, E., Petersen, N. H., Nylandsted, J., and Jäättelä, M. (2012) Identification of cytoskeleton-associated proteins essential for lysosomal stability and survival of human cancer cells. *PLoS One* **7,** e45381 CrossRef Medline
62. Hancock, W. O. (2014) Bidirectional cargo transport: moving beyond tug of war. *Nat. Rev. Mol. Cell Biol.* **15,** 615–628 CrossRef Medline
63. Lucanus, A. J., and Yip, G. W. (2018) Kinesin superfamily: roles in breast cancer, patient prognosis and therapeutics. *Oncogene* **37,** 833–838 CrossRef Medline
64. Kasahara, M., Nagahara, M., Nakagawa, T., Ishikawa, T., Sato, T., Uetake, H., and Sugihara, K. (2016) Clinicopathological relevance of kinesin family member 18A expression in invasive breast cancer. *Oncol. Lett.* **12,** 1909–1914 CrossRef Medline
65. Miki, H., Setou, M., Kaneshiro, K., and Hirokawa, N. (2001) All kinesin superfamily protein, KIF, genes in mouse and human. *Proc. Natl. Acad. Sci. U.S.A.* **98,** 7004–7011 CrossRef Medline
66. Couto, C. A., Wang, H. Y., Green, J. C., Kiely, R., Siddaway, R., Borer, C., Pears, C. J., and Lakin, N. D. (2011) PARP regulates nonhomologous end joining through retention of Ku at double-strand breaks. *J. Cell Biol.* **194,** 367–375 CrossRef Medline
67. Rauch, J., Volinsky, N., Romano, D., and Kolch, W. (2011) The secret life of kinases: functions beyond catalysis. *Cell Commun. Signal.* **9,** 23 CrossRef Medline
68. Grossman, E. N., Giurumescu, C. A., and Chisholm, A. D. (2013) Mechanisms of ephrin receptor protein kinase-independent signaling in amphid axon guidance in *Caenorhabditis elegans*. *Genetics* **195,** 899–913 CrossRef Medline
69. Ortiz-Zapater, E., Lee, R. W., Owen, W., Weitsman, G., Fruhwirth, G., Dunn, R. G., Neat, M. J., McCaughan, F., Parker, P., Ng, T., and Santis, G. (2017) MET-EGFR dimerization in lung adenocarcinoma is dependent on EGFR mtations and altered by MET kinase inhibition. *PLoS One* **12,** e0170798 CrossRef Medline
70. Chae, Y. K., Gagliato Dde, M., Pai, S. G., Carneiro, B., Mohindra, N., Giles, F. J., Ramakrishnan-Geethakumari, P., Sohn, J., Liu, S., Chen, H., Ueno, N., Hortobagyi, G., and Gonzalez-Angulo, A. M. (2016) The association between EGFR and cMET expression and phosphorylation and its prognostic implication in patients with breast cancer. *PLoS One* **11,** e0152585 CrossRef Medline
71. Romano, P., Manniello, A., Aresu, O., Armento, M., Cesaro, M., and Parodi, B. (2009) Cell Line Data Base: structure and recent improvements towards molecular authentication of human cell lines. *Nucleic Acids Res.* **37,** D925–D932 CrossRef Medline

H_2O_2 induces nuclear transport of the receptor tyrosine kinase c-MET in breast cancer cells via a membrane-bound retrograde trafficking mechanism

Mei-Kuang Chen, Yi Du, Linlin Sun, Jennifer L. Hsu, Yu-Han Wang, Yuan Gao, Jiaxing Huang and Mien-Chie Hung

J. Biol. Chem. 2019, 294:8516-8528.
doi: 10.1074/jbc.RA118.005953 originally published online April 8, 2019